

1
2
3
4
5
6
7
8
9
10
11
12
13
14
15
16
17
18
19
20
21
22
23
24
25
26
27
28
29
30
31
32
33
34
35
36
37
38
39
40
41
42
43
44
45
46
47
48
49
50
51
52
53
54
55
56
57
58
59
60
61
62
63
64
65

Morphodynamical Modelling of Field-Scale Swash Events

Giorgio Incelli^{a,*}, Nicholas Dodd^a, Chris E. Blenkinsopp^b, Fangfang Zhu^c,
Riccardo Briganti^a

^aUniversity of Nottingham, Faculty of Engineering, University Park, Nottingham, NG7
2RD, UK

^bUniversity of Bath, Department of Architecture and Civil Engineering, Claverton Down,
Bath, BA2 7AY, UK

^cUniversity of Nottingham Ningbo Campus, Department of Civil Engineering, 199 Taikang
East Road, Ningbo, 315100, China

Abstract

In the present work, measurements for three single swash events are selected from those available for an accretive tide that occurred at Le Truc Vert beach (France) during a field campaign at that location. These data are compared to results obtained from a ‘state-of-the art’ numerical fully-coupled 1D morphodynamical shallow water solver, driven by measurements made of those events in the lower swash / inner surf zone.

It is found that the hydrodynamics is reasonably well represented, although the computed results exhibit reduced maximum inundations in comparison with the observed ones. The model reproduces the correct order of magnitude of the morphodynamic change after each event, and sometimes the pattern of erosion and deposition, but this change is generally underestimated.

Sensitivity analyses are conducted with respect to more uncertain physical parameters and assumed initial conditions. They suggest that initial spatial distributions for velocity and pre-suspended sediment concentration play a key role in the quantitative and qualitative prediction of the bed change.

Keywords: single swash event, swash zone sediment transport, shallow water flows, fully-coupled morphodynamics, field / model comparison

*Corresponding author
Email address: evxgi1@nottingham.ac.uk ()

1
2
3
4
5
6
7
8
9 **1. Introduction**

10 Research into how best numerically to reproduce observed swash motions
11 dates back most obviously to the work of Hibberd & Peregrine (1979), in which
12 the flux-conservative form of the nonlinear shallow water equations (NSWEs)
13 were first proposed and used to simulate the inundation and subsequent drying
14 5 of a plane, immobile beach. Since then there has been much work on improved
15 numerical modelling using these equations (see e.g. Brocchini & Dodd, 2008),
16 research using more comprehensive hydrodynamic descriptions (see e.g. Zhang
17 & Liu, 2008), and work in which other physical effects have been considered,
18 such as infiltration of water into the beach during the event, including the escape
19 10 of air from the void space (Steenhauer et al., 2012), and, of course, the mobility
20 of the beach itself (see e.g. Briganti et al., 2012a; Postacchini et al., 2012). In
21 validation of the accuracy of these approaches extensive use has been made of
22 data-sets of swash motions in the laboratory (see e.g. O’Donoghue et al., 2010;
23 Briganti et al., 2012b).
24 15

25 So far, however, there have been few attempts to reproduce observed motions
26 in the field. There are good reasons for this. On a real beach motions
27 can be significantly three dimensional, therefore ideally requiring a correspond-
28 ing mathematical description. Linked to this is the corresponding difficulty
29 in adequately prescribing wave conditions further offshore so as to achieve a
30 20 good reproduction within the swash, and in accurately measuring the beach
31 evolution over an area. Nonetheless, because beach levels primarily vary in the
32 offshore direction, and because wave refraction turns wave directions so as to be
33 shore-normal as the swash is approached, it is reasonable to suppose that a 1D
34 description (i.e. cross-shore independent variable only, plus time) can reproduce
35 25 conditions on some beaches, for some data-sets. Such an attempt to test this
36 hypothesis was made by Van Rooijen et al. (2012), who used a model based on
37 the NSWEs (including a diffusion term, simulating energy dissipation through
38 horizontal eddies, in addition to energy loss due directly to breaking), linked
39 to suspended load and bed change equations, and driven by measured water
40 30 levels in about 1 to 1.5 m depth of water (in the inner surf zone) to drive swash
41 motions at the beachface. Simulations were performed over two high tides (one
42 accretive, 3 hours; and one erosive, 6 hours). Water depths predicted by these
43 simulations were compared with those measured (at Le Truc Vert beach, on the
44 Atlantic French coast (Blenkinsopp et al., 2011)) during the same experiments.
45 35 The results obtained were promising in some regard, both in terms of repro-
46 ducing signals of water depths and also of net bed change. Discrepancies are
47 nonetheless sometimes substantial, and Van Rooijen et al. (2012) attribute this
48 mainly to the effect of spatial inhomogeneity along the beach.
49

50 The purpose of the present contribution is to undertake a similar study,
51 40 but this time to focus on individual swash events only, in the swash zone only.
52 Specifically, we wish to determine whether water depths, velocities and bed
53 changes can be accurately reproduced with this modelling approach driven by
54 the level of detail provided by the measurements made in a comprehensive field
55 campaign, both in terms of time series and parametric values.
56 45
57
58
59
60
61
62
63
64
65

1
2
3
4
5
6
7
8
9 **2. Field campaign and selected events**

10
11 *2.1. Study site*

12 We make use of the same data-set as that used by Van Rooijen et al. (2012).
13 This data-set was specifically collected to enable the analysis of swash hydro-
14 dynamics and sediment transport at the timescale of individual waves and was
15 50 obtained at Le Truc Vert, France. The experiment described here was com-
16 pleted over a spring to spring tidal cycle from 19th March to 4th April as part
17 of the ECORS project (Sénéchal & Ardhuin, 2008).

18 Le Truc Vert is a long west-facing sandy beach on the Atlantic coast of France.
19 The beach is relatively steep with a typical gradient of approximately 1:15 and
20 55 median sediment grain size of approximately 0.4×10^{-3} m. It has a spring tidal
21 range of 4.3 m and is exposed to energetic swell and locally generated wind
22 waves with an average significant wave height of 1.3 m (De Melo Apoluceno
23 et al., 2002). During the experimental campaign, wave conditions were mea-
24 60 sured by a Waverider buoy installed in approximately 20 m of water offshore of
25 the site, with the significant wave height and period in the range 0.9 m to 4.1
26 m and 5 s to 13 s respectively.

27 The data examined in this paper were obtained over the morning high tide on
28 26th March, which was thought to provide suitable, quasi-1D swash events (note
29 65 that the tides examined by Van Rooijen et al. (2012) were on March 20th and
30 21st). During this high tide mean offshore significant wave height and mean
31 peak wave period were 1.72 m and 9.4 s respectively, and the mean nearshore
32 significant wave height measured using a bed-mounted pressure transducer lo-
33 cated in the surf zone was 0.55 m. Morphological change during this period was
34 70 characterised by moderate accretion (Fig. 1), particularly during the rising tide
35 which caused an increase in the beach volume of $0.54 \text{ m}^3/\text{m}$ landward of the
36 high tide surf / swash boundary.
37
38

39 *2.2. Instrumentation*

40 A total of 89 sensors were installed on the beach face to measure a range of
41 75 hydrodynamic and morphodynamic parameters around high tide over 28 tidal
42 cycles. The description of instrumentation below focusses on the sensors used
43 to collect the data utilised in the current study. A complete description of the
44 instrumentation deployed during the experiment can be found in Masselink et al.
45 (2009).
46

47 80 To obtain bed elevation (z_b) and swash surface data ($h + z_b$, where h is
48 the water depth) on a wave-by-wave basis throughout the swash zone, an array
49 of ultrasonic altimeters (Massa M300/95) were deployed in three, 26.6 m long
50 cross-shore lines of 15 sensors (longshore separation of 1.9 m) on a scaffold
51 frame (see Fig. 2). The sensors (we henceforth use the terms “sensor” and
52 85 “altimeter” interchangeably, distinguishing these devices from the stations and
53 transducers and meters—see below) were mounted at 1.9 m cross-shore spacing
54 approximately 1 m above the bed. As described by Turner et al. (2008), when
55 mounted perpendicular to the bed, the ultrasonic altimeters use the time of
56 flight of a reflected signal to obtain non-intrusive Eulerian measurements of the
57
58

1
2
3
4
5
6
7
8
9
10
11
12
13
14
15
16
17
18
19
20
21
22
23
24
25
26
27
28
29
30
31
32
33
34
35
36
37
38
39
40
41
42
43
44
45
46
47
48
49
50
51
52
53
54
55
56
57
58
59
60
61
62
63
64
65

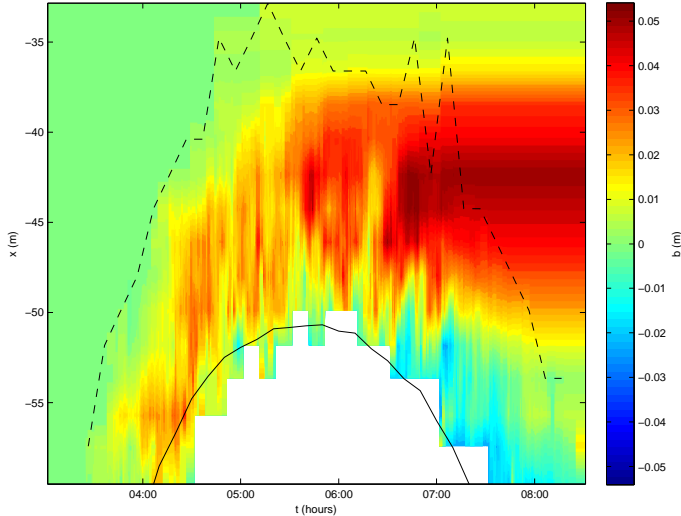


Figure 1: Change in bed elevation (b) within the swash zone during the morning high tide of 26th March, 2008 measured using the array of ultrasonic altimeters (see Section 2.2). The dashed and solid lines represent the run-up limit and the intersection of the beach and mean sea level respectively. The colour scheme represents the change in bed elevation relative to the beach face morphology at the start of the time series.

vertical distance to the closest target: sand when the bed is dry and the swash surface when the bed is wet. Thus through careful post-processing, the elevation of the bed or swash surface elevation relative to the local datum can be obtained at multiple locations within the swash zone at the sample frequency of 4 Hz. As described by Blenkinsopp et al. (2011), the data recorded by each of the three cross-shore lines of sensors were almost identical and as a result, only data from the central line are used in the current study. Therefore, there are 15 sensors distributed across the region of interest in our study, numbered 1 to 15, from offshore to nearshore (see Fig. 2).

Flow velocities were measured at five instrument stations located at 3.8 m intervals along the centre of the scaffold frame. The main instrument station was installed in the mid high tide swash zone ($x = -52.1$ m), almost co-located with an ultrasonic altimeter. The station was equipped with four Valeport electromagnetic current meters which are able to measure swash flow velocity in both the long and cross-shore directions at elevations 0.03 m, 0.06 m, 0.10 m and 0.14 m above the local bed. Additionally, three Druck PTX1830 pressure transducers provided measurements of water depth to compare with those derived from altimeter data. Further four auxiliary stations were installed both landward and seaward of the main instrument station at cross-shore locations $x = -44.5$ m, -48.3 m, -55.8 m and -59.7 m. These were each equipped with a single electromagnetic current meter deployed 0.06 m above the bed and a pressure

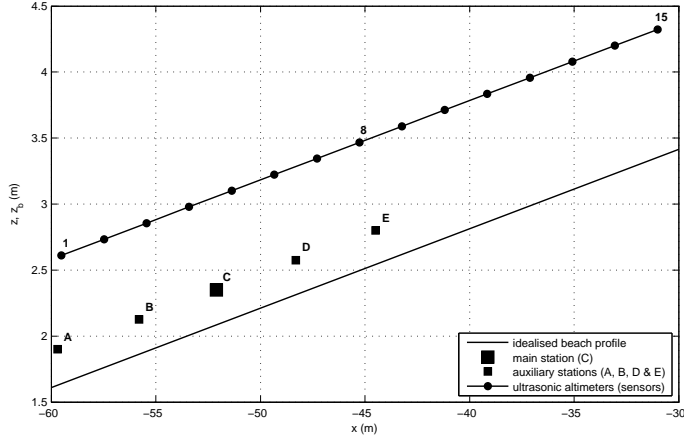


Figure 2: Schematic showing the instrument locations during 26th March, 2008.

transducer (0.03 m above the bed). For our purposes we refer to these stations as A (-59.7 m) to E (-44.5 m) in Fig. 2. It is noted that on 26th March, the electromagnetic current meters at auxiliary stations A and E were not working and thus are not used in the current study.

115 2.3. Selected events

Three events, referred to here with a numbering system that reflects the original number considered, are denoted Event 1, 3 and 5, and are selected from the data for the aforementioned tide. They are all single swash events—although sometimes comprising more than one wave / bore—of a reasonable duration (20-30 s), and are firstly selected because of the different kind of final bed change profile they produced. Event 1 generated variable accretion in most of the swash zone; Event 3 caused significant erosion in the lower swash zone but accretion in the upper part; and Event 5 yielded an erosional profile, particularly apparent in the lower swash zone. Secondly, these events are chosen because complete (or nearly complete) time series for water depth and velocity are available at sensor 3 / station B ($x_3 = -55.7$ m / $x_B = -55.8$ m), which are located at almost the same position (see Fig. 2). These time series are needed as inputs at the seaward boundary for numerical simulations. Typically, complete velocity time series are not always available.

130 The initial time for each event is defined such that the initial shoreline ($x_s(t = t_0)$) is at sensor 6 ($x_6 = -49.9$ m), where water depth is therefore set to zero, following the approach to detect a dried bed described in Blenkinsopp et al. (2011). This choice of relating the initial time to a shoreline location at sensor 6 is somewhat arbitrary but coincided for both Events 3 and 5 with a time at which velocity time series exist after a sequence of unrecorded values. 135 The same approach is retained for consistency for Event 1.

1
2
3
4
5
6
7
8
9
10
11
12
13
14
15
16
17
18
19
20
21
22
23
24
25
26
27
28
29
30
31
32
33
34
35
36
37
38
39
40
41
42
43
44
45
46
47
48
49
50
51
52
53
54
55
56
57
58
59
60
61
62
63
64
65

The duration of each event is limited to a few seconds after the time that $x_s(t)$ retreats seaward of $x_s(t_0)$, in order to be confident that the beachface has returned to a dry state. This allows consistent comparison between initial and final bed profiles and therefore the computation of the measured final bed change profile.

1
2
3
4
5
6
7
8
9 **3. Numerical modelling**

10
11 *3.1. Numerical model*

12 The numerical model used originates from the TVD-MacCormack solver
13 presented in Briganti et al. (2012a) and comprises the bottom boundary layer
14 description from Briganti et al. (2011).

15 Additionally, this new version of the model includes a bed diffusion mechanism,
16 obtained through a downslope correction to the bedload sediment transport for-
17 mula and the infiltration model of Packwood (1983). The last two developments
18 are implemented following Dodd et al. (2008).
19

20 Furthermore, suspended sediment transport is considered, according to the ap-
21 proach presented in Zhu & Dodd (2015). The original NSWEs-Exner system is
22 extended with an additional equation for the suspended sediment conservation,
23 maintaining the conservative form and the fully-coupled character of the solver
24 (see Zhu, 2012, for derivation). A brief description of the governing equations
25 and of the numerical model are provided in Appendix A and in Appendix B
26 respectively.
27

28 *3.2. Modelling approach*

29 As mentioned, the actual swash events, including the beach itself, show
30 alongshore variation, but measurements at adjacent alongshore sensor locations
31 confirm the predominant cross-shore character of swash zone sediment transport
32 at the field site during the campaign (Blenkinsopp et al., 2011). This observation
33 allows us a reasonable expectation that use of the above-mentioned 1D numerical
34 model is appropriate, provided that some loss of accuracy in the computed
35 results compared to the field data is acknowledged.
36

37
38 *3.2.1. Boundary conditions*

39 As mentioned, the driving seaward boundary is located at x_3 ($\approx x_B$), where
40 the boundary time series for h and velocity (u) are available. Note that only
41 at the main station (C) can we estimate the depth-averaged velocity from the
42 measurements, because of the multiple measurements of velocity over the water
43 column. However, we here interpret measured velocity values from station B
44 (0.06 m above the bed) as depth-averaged. The prototype scale measurements
45 of Briganti et al. (2011) provide justification for this in the uprush. In the
46 backwash there is some evidence that doing so will result in an overestimate of
47 the depth-averaged value. Further comments on this point are provided later
48 (see Section 3.5). Sometimes, especially when water depth becomes small and a
49 previous significant backwash meets the subsequent uprush, the water velocity
50 time series are incomplete in the later stages of the events. When required,
51 gaps in the time series are filled with values obtained through a piecewise cubic
52 interpolation from adjacent values. Note also that because single swash events
53 only are considered, the accumulated effects of interpolations are assumed small.
54 Example time series (h and u for Event 1) are shown in Fig. 3. Note that
55 hereafter we use the symbol u to refer interchangeably to depth-averaged and
56
57
58
59
60
61
62
63
64
65

(measured) instantaneous values, only distinguishing between these quantities
 185 as necessary.

No corresponding boundary information for z_b and concentration (depth-
 averaged, C , or otherwise) is available at the seaward boundary. Bed levels at
 sensor 3 / station B could, in theory, be calculated by subtracting estimates
 of h (from the pressure transducer at station B) from those of water surface
 190 (from the altimeter that is sensor 3—notwithstanding the small discrepancy in
 station / sensor positions there), but the loss of accuracy accompanying this
 was deemed unacceptable. Therefore, two different approaches were employed,
 the first not to update bed level and concentration at the the driving boundary,
 and the second to extrapolate them from the nearest internal point. Both these
 195 approaches led to very similar predictions for bed changes at a distance > 1 m
 away from the driving boundary. Therefore the first of these was used here.

Note that the driving signals therefore, in theory, include both incoming
 and reflected components, contrary to the driving signals of Van Rooijen et al.
 (2012). Recall, however, that we are driving our model from the base of the
 200 swash zone, where disentangling these two signals from field data is more diffi-
 cult, and that the uprush (backwash) for the events we consider will primarily
 consist of shoreward (seaward) propagating component, exclusively so if flow is
 supercritical. Lastly, because the spatial dimension and (especially) time dura-
 tions are considerably reduced, we may expect that this approach will also lead
 205 to fewer discrepancies because there is no accumulation.

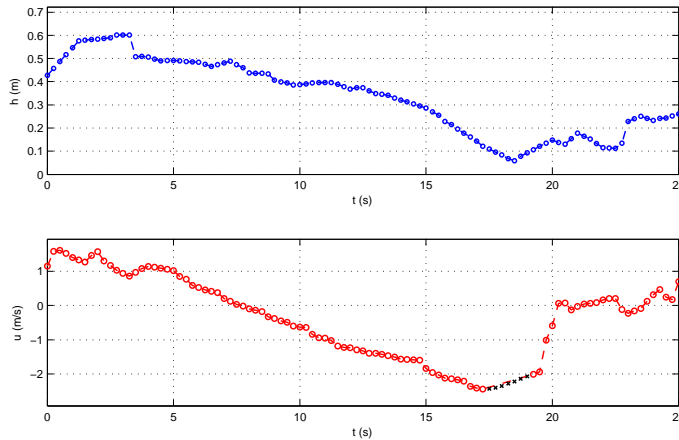


Figure 3: Event 1. Boundary time series. Top panel: water depth (h); bottom panel: water
 velocity (u) (black crosses indicate interpolated values).

3.2.2. Initial conditions

In the initially dry part of the beach, sensors provide values for the bed
 levels. In the initially wet part, they return the levels of the water surface and
 the water depths are then computed by subtracting the bed levels recovered from

1
2
3
4
5
6
7
8
9
10
11
12
13
14
15
16
17
18
19
20
21
22
23
24
25
26
27
28
29
30
31
32
33
34
35
36
37
38
39
40
41
42
43
44
45
46
47
48
49
50
51
52
53
54
55
56
57
58
59
60
61
62
63
64
65

210 the previous time when the bed was exposed at these locations. At numerical grid points between sensor locations linear interpolation was used to estimate z_b and h , using values from sensor locations.

Initial velocities are not available at all locations, so a spatial distribution is constructed by linear interpolation between the initial value at the seaward boundary $u(x_B, t_0)$ and that estimated at the initial shoreline ($u(x_s(t_0))$). The latter is calculated by evaluating the time interval for the shoreline, x_s , initially at $x = x_6$ recall, to reach the first sensor further landward (sensor 7, or equivalently its location x_7). Note also that measurements for velocity at the station (C) location were also not available at $t = t_0$. Because no reliable or cross-shore measurements of C are available, a zero depth-averaged concentration ($C(x, t = t_0) = 0$) was imposed everywhere. The sensitivity to this assumption is examined later.

Because of lack of knowledge, the initial boundary layer thickness was set to zero (no boundary layer present), which then rapidly developed as solution progressed.

Measurements concerning the water table level within the beach also were not available. It was therefore assumed that the water table level is equal to the bed level at the initial shoreline, i.e. to $z_b(x_s(t_0)) = z_b(x_6, t_0)$.

3.3. Parameter settings

230 The bed porosity is $p_b = 0.35$, the relative sediment density compared to salted water $s_{rel} = 2.580$ (sediment density $\rho_s = 2650 \text{ kg/m}^3$, salted water density $\rho_w = 1027 \text{ kg/m}^3$), and the median sediment diameter $d_{50} = 0.4 \times 10^{-3} \text{ m}$ (Blenkinsopp et al., 2011). The critical Shields parameter for bedload motion is $\theta_{crb} \approx 3.6 \times 10^{-2}$, following Soulsby (1997) and Van Rijn (2007). As the beach sediment is a medium grain size, the angle of repose of sediment $\phi = 33^\circ$ is assumed.

For suspended load sediment transport, the effective settling velocity $w_s = 0.05 \text{ m/s}$ is imposed (Blenkinsopp et al., 2011), while the critical friction velocity for suspended load $u_{f,crs} = \sqrt{\tau_{crs}/\rho_w} \approx 2.5 \times 10^{-2} \text{ m/s}$ (Van Rijn, 1984). It is more difficult to estimate the parameter for the erosional rate m_e and the reference bed shear stress value τ_0 . Zhu & Dodd (2015) make an attempt to find a relationship between erosional and depositional rates for given net on-shore flux of sediment entrained in the uprush only of a solitary wave swash event. Although it is difficult to understand to what extent those results can be applied to the present field case, they suggest a reasonable range of values for the non-dimensional parameter $M = m_e / (\sqrt{gh_0}(1 - p_b))$. Our choice is $m_e = 2 \times 10^{-3} \text{ m/s}$, which corresponds to $M = 1 \times 10^{-3}$, where a representative depth $h_0 = 1 \text{ m}$ has been used. The sensitivity to this assumption is examined later. Additionally, here we take $\tau_0 = \rho_w c_d u^2$, and $c_d = 5 \times 10^{-3}$. This value for c_d is found through a preliminary model calibration (not shown) undertaken 240 for c_d is found through a preliminary model calibration (not shown) undertaken running simulations with a Chézy approach (i.e. fixed drag coefficient) for friction description instead of the bottom boundary layer solver. Note, however, that this is only for the purposes of estimating τ_0 : the boundary layer submodel provides values of τ_b used in the modelling.

1
2
3
4
5
6
7
8
9
255 In the bottom boundary layer solver an estimate for the bed roughness K_n is needed. Its value is usually related to sediment grain sizes at various percentiles (see Van Rijn, 1982, among others). Following previous work of Van Rooijen et al. (2012), it is here assumed that $K_n = 2.5d_{50} = 1.0 \times 10^{-3}$ m.

10
11
12
13 To simulate infiltration, a hydraulic conductivity of the sediment K_{hyd} of
14
260 1×10^{-3} m/s is employed, following the guidance for medium sand proposed by Packwood & Peregrine (1980).

15
16 Finally, we use a spatial step size $\Delta x = 1 \times 10^{-2}$ m, a Courant Number
17 $C_N = 0.5$, and a minimum water depth $h_{min} = 1 \times 10^{-3}$ m. The latter value
18 appears to be a reasonable one as it agrees with the measured data vertical
19
265 resolution.

21 22 *3.4. Simulation results*

23 In this section, results for each event are presented, including a brief descrip-
24 tion of both hydrodynamics and morphodynamics.

27 28 *3.4.1. Event 1*

29 Fig. 4 shows the images for dependent variables for Event 1. The hydro-
30 dynamics present a large event generated by a single bore. The water retreats
31 slowly as a thin film in the backwash, due to the effect of friction. Bed change
32 contours display some deposition in the upper swash with significant erosion
275 in the lower swash zone. Suspended sediment concentration increases rapidly
33 in the uprush phase, drops at flow reversal and peaks again in late backwash,
34 consistently with the development of the bottom boundary layer.

35
36 Fig. 5 presents the time stack for the cumulative infiltrated volume of water
37 per unit width (V_{inf}). The final volume of percolated water is $0.418 \text{ m}^3/\text{m}$,
38 which corresponds to approximately the 15.7% of the total volume that enters
280 the region landward of the initial shoreline ($x > x_6 = x_s(t_0)$) during the
39 simulation.
40

42 43 *3.4.2. Event 3*

44 Fig. 6 shows the timestacks for dependent variables for Event 3. The swash
285 event is produced by two subsequent bores. The second one reaches its maxi-
45 mum runup while water from the first one already started receding. Significant
46 deposition in the upper swash and noticeable erosion in the lower swash zone
47 are highlighted by the bed change contours. Suspended sediment concentration
48 rises quickly in the uprush phase, reaching values greater than twice the maxi-
49 mum ones in Event 1, indicating that Event 3 is much more energetic than the
290 previous one. Evolution of C then follows the same behaviour as for Event 1.

51 The equivalent plot for V_{inf} is not shown here because it is qualitatively
52 similar to that for Event 1. The final volume of percolated water is $0.427 \text{ m}^3/\text{m}$
53 (16.9% of water entering the region landward of the initial shoreline).
54
55
56
57
58

1
2
3
4
5
6
7
8
9
10
11
12
13
14
15
16
17
18
19
20
21
22
23
24
25
26
27
28
29
30
31
32
33
34
35
36
37
38
39
40
41
42
43
44
45
46
47
48
49
50
51
52
53
54
55
56
57
58
59
60
61
62
63
64
65

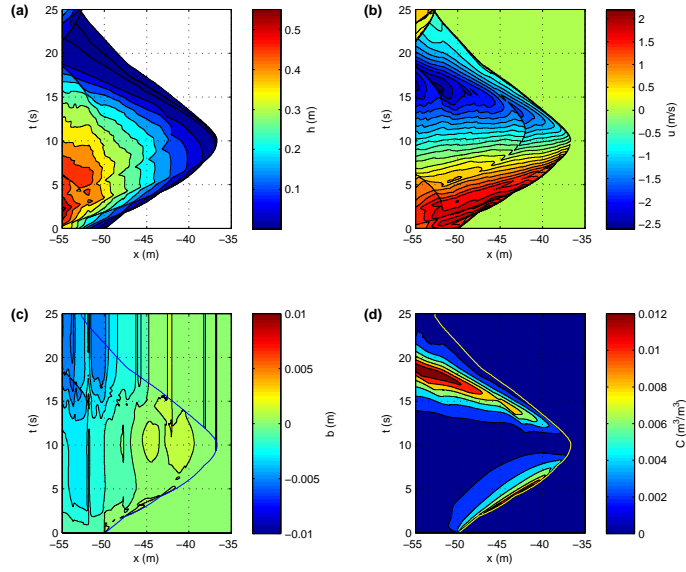


Figure 4: Event 1. Timestacks. Panels: (a) water depth (h); (b) water velocity (u); (c) bed change (b); (d) suspended sediment concentration (C). A line tracking the numerical shoreline is added for convenience in panels (c) and (d) in blue and yellow respectively.

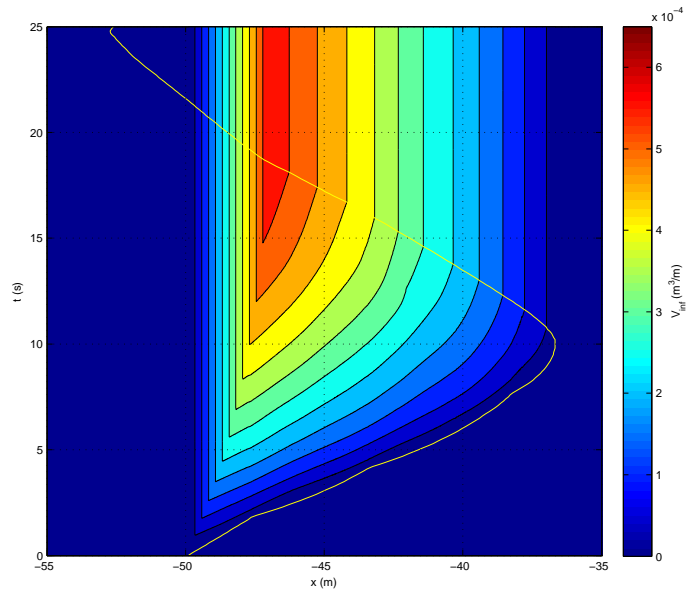


Figure 5: Event 1. Timestack for cumulative volume of percolated water (V_{inf}). A yellow line tracking the numerical shoreline is added for convenience.

1
2
3
4
5
6
7
8
9
10
11
12
13
14
15
16
17
18
19
20
21
22
23
24
25
26
27
28
29
30
31
32
33
34
35
36
37
38
39
40
41
42
43
44
45
46
47
48
49
50
51
52
53
54
55
56
57
58
59
60
61
62
63
64
65

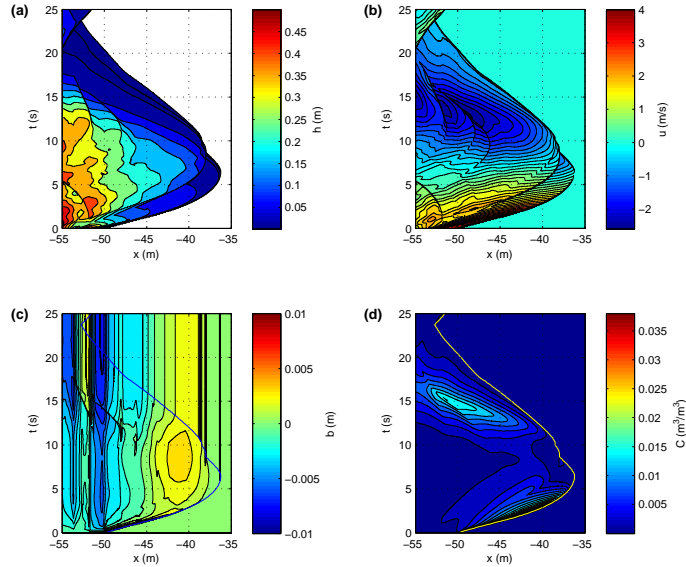


Figure 6: Event 3. Timestacks. Panels: (a) water depth (h); (b) water velocity (u); (c) bed change (b); (d) suspended sediment concentration (C). A line tracking the numerical shoreline is added for convenience in panels (c) and (d) in blue and yellow respectively.

295 3.4.3. Event 5

Three consecutive bores, the first of them smaller than the following two, are included in Event 5 (Fig. 7). Little accretion is observed in the upper swash while erosion is apparent in the lower swash zone. The first bore produces no significant amount of suspended sediment transport. Then suspended load increases during uprush and backwash phases of the other bores and hits its maximum concentration in the last backwash phase.

Fig. 8 shows once more the infiltration, with the three bores apparent. The final volume of percolated water is $0.329 \text{ m}^3/\text{m}$ (16.6%). This relatively small volume of water, compared to the other two events, could be caused by the smaller maximum run-up in the present event, which means reduced time and pore space available for infiltration.

3.5. Comparison with data

In this section, comparisons between data and numerical results are shown in terms of surface levels, water velocities and final bed changes.

Figs. 9, 10 and 11 show comparisons between the computed surface levels predicted by the model and measured ones for Events 1, 3 and 5 respectively. The numerical results compare quite well to the measured data in all three events, notwithstanding all the uncertainties mentioned in Section 3.2. All simulated events exhibit smaller maximum run-ups, in particular Event 3. The ‘missing’ water depth at the tip of the swash lens is never more than 0.06 m and

1
2
3
4
5
6
7
8
9
10
11
12
13
14
15
16
17
18
19
20
21
22
23
24
25
26
27
28
29
30
31
32
33
34
35
36
37
38
39
40
41
42
43
44
45
46
47
48
49
50
51
52
53
54
55
56
57
58
59
60
61
62
63
64
65

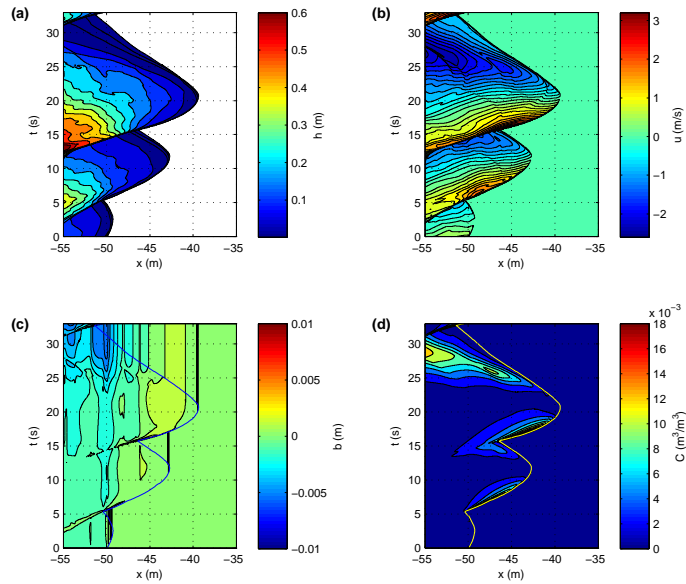


Figure 7: Event 5. Timestacks. Panels: (a) water depth (h); (b) water velocity (u); (c) bed change (b); (d) suspended sediment concentration (C). A line tracking the numerical shoreline is added for convenience in panels (c) and (d) in blue and yellow respectively.

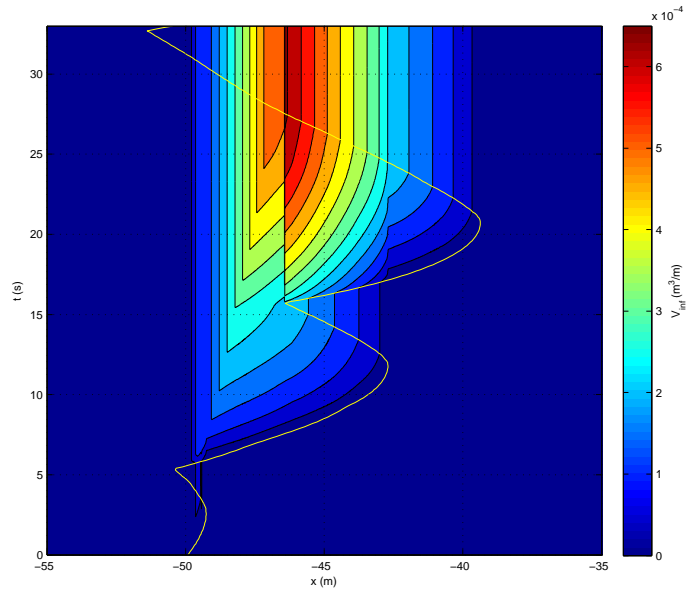


Figure 8: Event 5. Timestack for cumulative volume of percolated water (V_{inf}). A yellow line tracking the numerical shoreline is added for convenience.

generally around 0.03 m. For Events 1 and 5, some lag in the uprush phases can be observed starting from lower sensor locations and increasing slightly landward. This lag can be noticed in the backwash phases of both events as well, but to a smaller extent. Note, however, that the reduced water in the upper swash results in the numerical signal leading the measured one on the backwash in the upper swash. On the other hand, nearly no lag can be seen for Event 3 in the uprush.

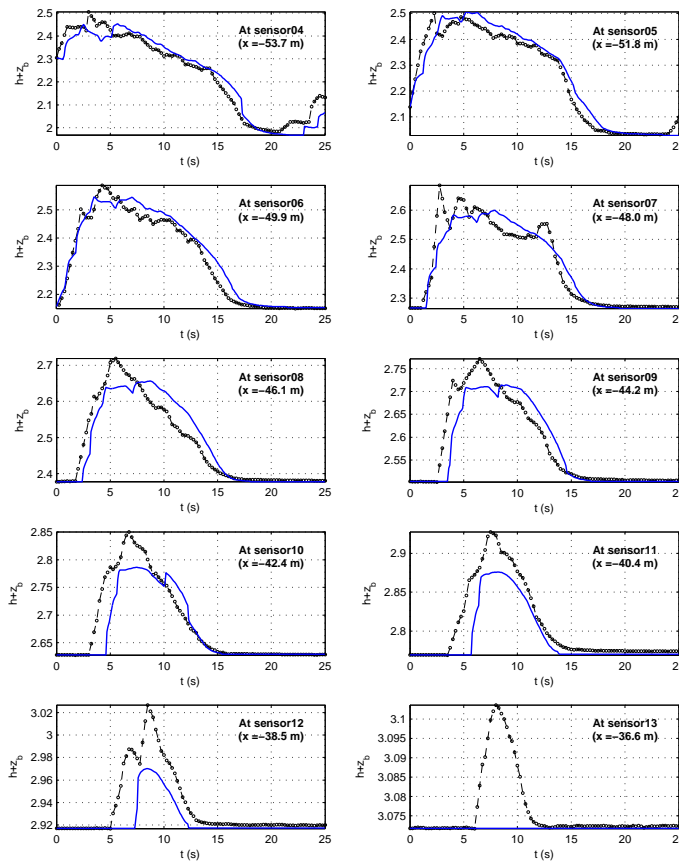


Figure 9: Event 1. Surface level comparisons. Dashed black line with circles: data. Solid blue line: computed results.

We make comparison with measured velocities at station C (the main station) when the station remains submerged for a long enough time to let velocity data be recorded by current meters (see Fig. 12). In theory, depth-averaged values for velocity could be calculated using estimates of h from the pressure transducer at station C, but, as noted in Section 3.2.1, loss of accuracy accompanying this could be unacceptable. The measured velocities at different elevations

1
2
3
4
5
6
7
8
9
10
11
12
13
14
15
16
17
18
19
20
21
22
23
24
25
26
27
28
29
30
31
32
33
34
35
36
37
38
39
40
41
42
43
44
45
46
47
48
49
50
51
52
53
54
55
56
57
58
59
60
61
62
63
64
65

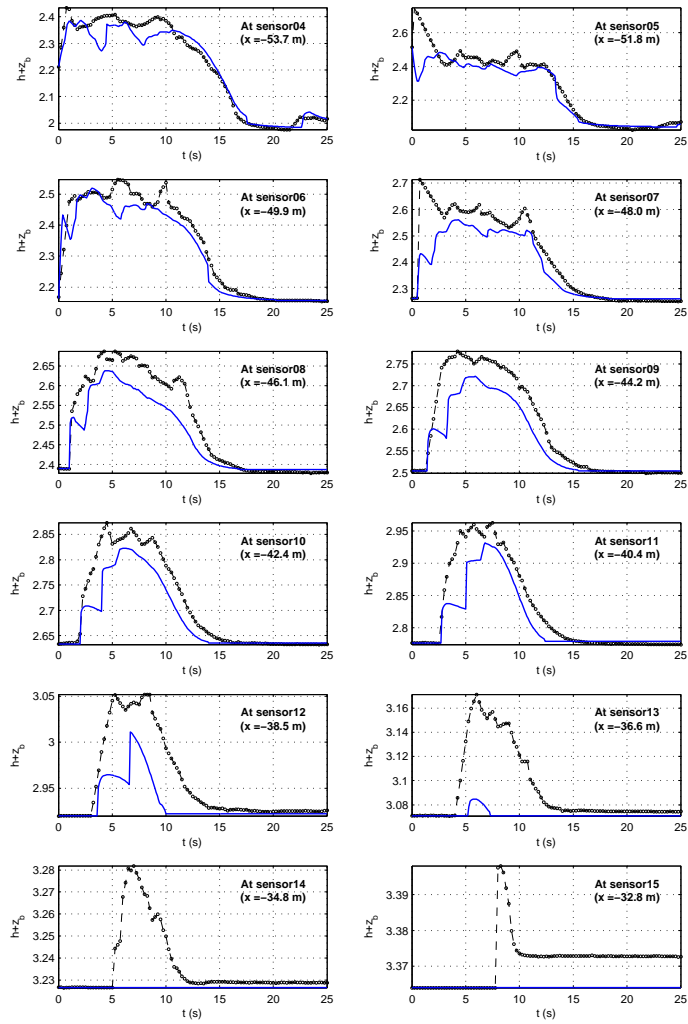


Figure 10: Event 3. Surface level comparisons. Dashed black line with circles: data. Solid blue line: computed results.

1
2
3
4
5
6
7
8
9
10
11
12
13
14
15
16
17
18
19
20
21
22
23
24
25
26
27
28
29
30
31
32
33
34
35
36
37
38
39
40
41
42
43
44
45
46
47
48
49
50
51
52
53
54
55
56
57
58
59
60
61
62
63
64
65

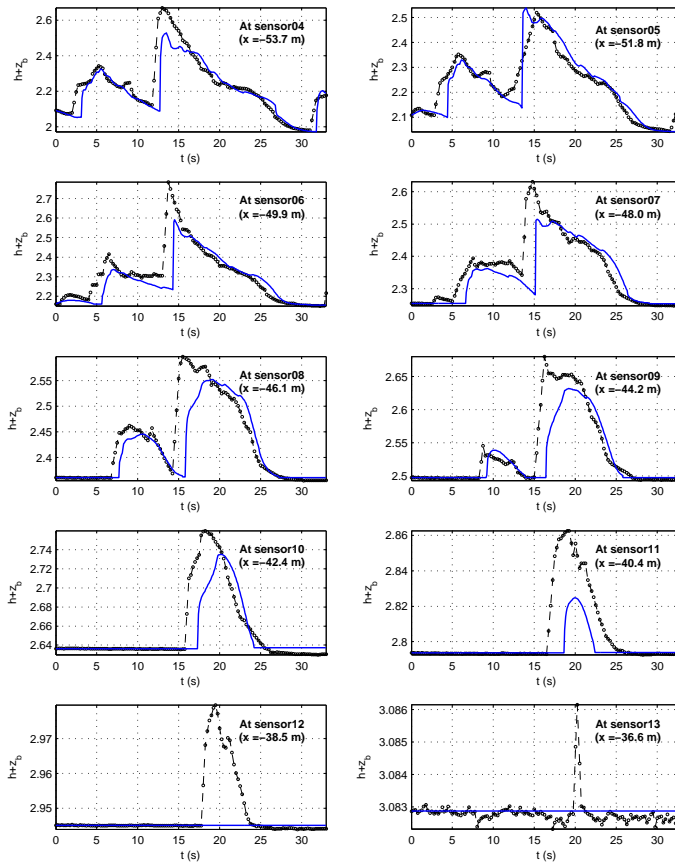


Figure 11: Event 5. Surface level comparisons. Dashed black line with circles: data. Solid blue line: computed results.

overall show similar values for most of the time series and are in general good agreement with the computed ones. This gives us an indication that our use of raw velocities (0.06 m above the bed, at station B; see Section 3.2.1) as depth-averaged driving boundary values nonetheless captures the physics reasonably well, and that, indeed, for most of the swash cycle depth-averaged velocities represent well values that measured over the water column.

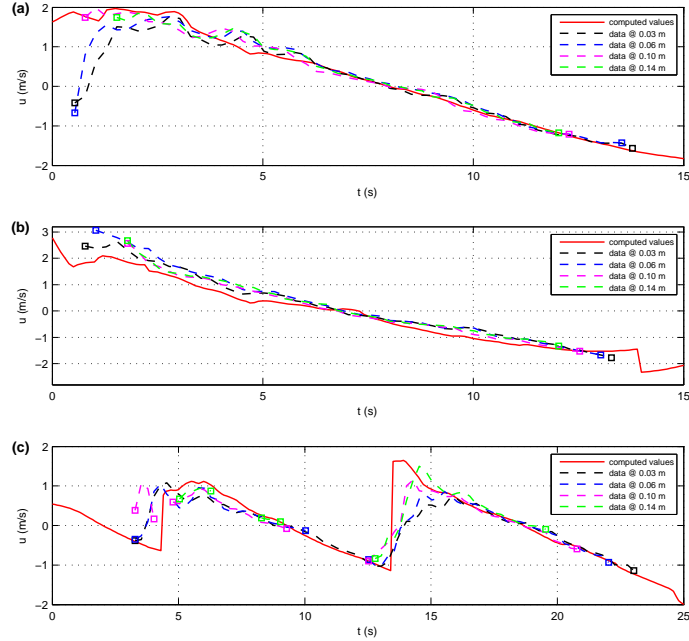


Figure 12: All events. Velocity comparisons at main station (C). Panels: (a) Event 1; (b) Event 3; (c) Event 5. Solid red line: computed depth-averaged velocity. Dashed black line: velocity data @ 0.03 m elevation. Dashed blue line: velocity data @ 0.06 m elevation. Dashed magenta line: velocity data @ 0.10 m elevation. Dashed green line: velocity data @ 0.14 m elevation. Squares, coloured accordingly to dashed lines, indicate first and last values of interval(s) of the measured time series with recorded values.

To appreciate the morphodynamic effects of the simulated swash events, final computed and measured bed changes are shown in Fig. 13 landward of the initial shoreline location. Considering this region ensures that all measured changes are due to the considered event only (recall that in the initially wet part of the domain, z_b values are recovered from previous time when the bed was exposed, therefore more uncertainty is related to them).

In Event 1, the computed deposition is much smaller than that measured, and some erosion is apparent in the lower swash zone. In Event 3, the numerical results seem to reproduce the overall morphodynamic pattern (i.e. erosion in the lower swash, deposition in the upper), although the amount of bed change is reduced. In particular, the reduced maximum run-up confines the accretion

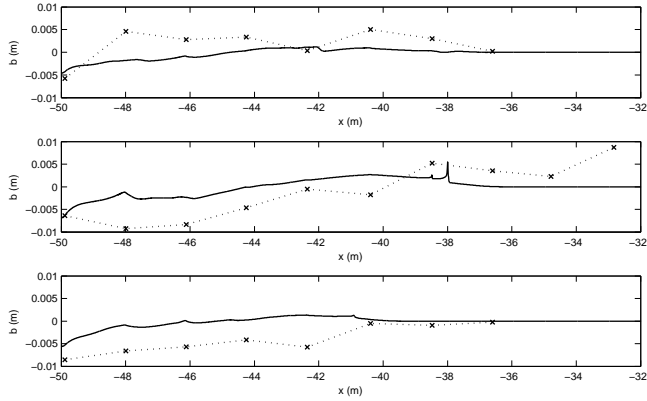


Figure 13: All events. Bed change comparisons. Panels: (a) Event 1; (b) Event 3; (c) Event 5. Dotted line with crosses: data at sensor locations. Solid line: computed results.

3.6. Sensitivity analyses

As mentioned, some elements of the modelling have little or no site data to provide estimates of initial conditions (C , u) or of parameter values (m_e , K_{hyd}). Other variables (h , z_b) and parameters (d_{50} , K_n , w_s , p_b , ϕ) are considered reasonably well prescribed. As has been noted, it could also be argued that boundary conditions for C and z_b are inadequately prescribed, but we again draw the reader's attention to the limited region of influence of $z_b(x_B, t)$ and $C(x_B, t)$ already described, at least for durations of the simulation of the order of the present ones. The work of Pritchard & Hogg (2005) and Zhu & Dodd (2015) also gives us some indication of the importance of $C(x, t = t_0)$ in influencing deposition and erosion in a swash event, such that we do not think that further alterations of $C(x_B, t)$ will make significant or at least qualitative changes. This must remain an unknown point, however.

To examine this sensitivity we focus on Event 3. We choose this event because (as can be seen in Fig. 13) there are significant changes (erosion and deposition) over most of the swash region in both simulation results and the field data.

3.6.1. Sensitivity to parameters

The parameter for the erosional rate m_e is the least well determined of all parameters and we turn to this first. Our original choice of m_e is 2×10^{-3} m/s. In Fig. 14 we show the effect of halving or doubling the m_e value (1×10^{-3} and

1
 2
 3
 4
 5
 6
 7
 8
 9
 10
 11
 12
 13
 14
 15
 16
 17
 18
 19
 20
 21
 22
 23
 24
 25
 26
 27
 28
 29
 30
 31
 32
 33
 34
 35
 36
 37
 38
 39
 40
 41
 42
 43
 44
 45
 46
 47
 48
 49
 50
 51
 52
 53
 54
 55
 56
 57
 58
 59
 60
 61
 62
 63
 64
 65

4×10^{-3} m/s respectively). It can be seen that the overall pattern of erosion / deposition is unchanged. This is consistent with Zhu & Dodd (2015), who also noted that this parameter affects primarily the amount of erosion / deposition (per unit time) rather than the pattern, unless the flow is significantly affected by the bed change (see (A.3)–(A.6)). These values of m_e span a range of M values from 5×10^{-4} – 2×10^{-3} (see Fig. 16 of Zhu & Dodd (2015)). The larger value corresponds to the uprush movement of around 60 kg/m of sand, which is consistent with field observations (see Blenkinsopp et al., 2011).

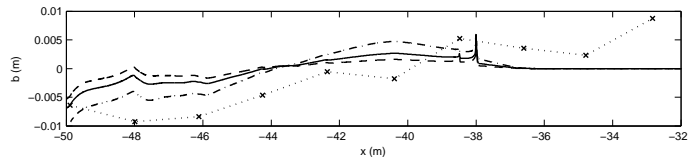


Figure 14: Event 3. Sensitivity of final bed change on the parameter for the erosional rate (m_e). Dotted line with crosses: data at sensor locations. Solid line: computed results with $m_e = 2 \times 10^{-3}$ m/s (reference case). Dashed line: computed results with $m_e = 1 \times 10^{-3}$ m/s. Dot-dash line: computed results with $m_e = 4 \times 10^{-3}$ m/s.

30
 31
 32
 33
 34
 35
 36
 37
 38
 39
 40
 41
 42
 43
 44
 45
 46
 47
 48
 49
 50
 51
 52
 53
 54
 55
 56
 57
 58
 59
 60
 61
 62
 63
 64
 65

Less uncertain is K_{hyd} . Nonetheless, it is difficult to obtain accurate values of this parameter. So, in Fig. 15 we compare reference results with those obtained for an impermeable beach. Both erosion in the lower swash and deposition in the upper swash increase, however from the morphodynamic viewpoint the difference is not substantial. Some improvements are observed in the hydrodynamics in terms of extended maximum run-up (not showed here), which allows for deposition to occur further landward.

Note that the value chosen as reference values for K_{hyd} results in highly uniform infiltrated volume percentages of between 15% and 17% of the water entering the region landward of the initial shoreline. These, for a sandy beach with $d_{50} = 0.4 \times 10^{-3}$ m, seem consistent with those values ($d_{50} = 1.3 \times 10^{-3}$ m, 33%) measured by Kikkert et al. (2013) in a flume.

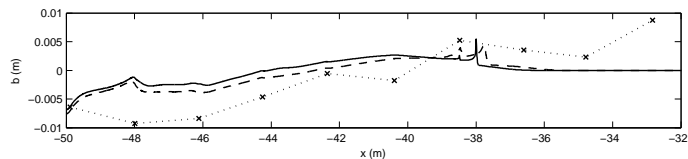


Figure 15: Event 3. Sensitivity of final bed change on infiltration. Dotted line with crosses: data at sensor locations. Solid line: computed results for permeable beach with $K_{hyd} = 1 \times 10^{-3}$ m/s (reference case). Dashed line: computed results for impermeable beach.

Finally, some other approximations for the bed roughness K_n were tested, but differences in the final morphodynamic change are negligible. These are not shown.

1
2
3
4
5
6
7
8
9
10
11
12
13
14
15
16
17
18
19
20
21
22
23
24
25
26
27
28
29
30
31
32
33
34
35
36
37
38
39
40
41
42
43
44
45
46
47
48
49
50
51
52
53
54
55
56
57
58
59
60
61
62
63
64
65

3.6.2. Sensitivity to initial conditions

395 The reconstruction procedure to obtain the initial water velocity profile
is described in Section 3.2. There is clearly scope for considerable variation
in $u(x, t_0)$. To account for this, by providing a markedly different but still
physically plausible $u(x, t_0)$ we proceed as follows. Instead of estimating a
non-zero velocity at the initial shoreline, $u(x_s(t_0))$ is set to zero there. Then
400 $u(x_B < x < x_s, t_0)$ values are (again) calculated by linear interpolation between
these two extremes.

Results for this new initial condition are shown in Fig. 16. The final bed change
profile loses nearly completely the depositional area in the upper swash, while
the erosional one is substantially reduced. The influence is therefore marked.

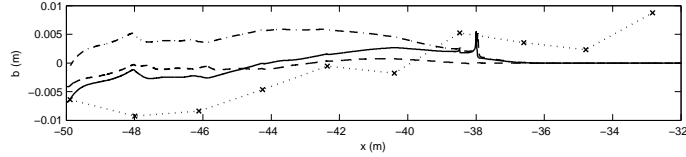


Figure 16: Event 3. Sensitivity of final bed change to initial velocity ($u(x, t_0)$) and concentration ($C(x, t_0)$) profiles. Dotted line with crosses: data at sensor locations. Solid line: computed results with increasing landward initial velocity profile and $C(x, t_0) = 0$ (reference case). Dashed line: computed results with decreasing landward initial velocity profile and $C(x, t_0) = 0$. Dot-dash line: computed results with increasing landward initial velocity profile and $C(x, t_0) = C_{eq}$.

In the same figure we illustrate the effect of assuming an initial equilibrium concentration profile $C(x, t_0) = C_{eq}$. This corresponds to a steady state profile where entrainment balances erosion, such that (see (A.6))

$$m_e \left(\frac{\tau_b - \tau_{crs}}{\tau_0} \right) - w_s C_{eq} = 0 \Rightarrow C_{eq} = \frac{m_e}{w_s} \left(\frac{c_d u^2 - u_{f,crs}^2}{\tau_0 / \rho_w} \right). \quad (1)$$

405 Results for this new initial condition are shown in Fig. 16. The presence of pre-suspended sediment removes all erosion from the final bed profile throughout the swash region. Effects of the new initial condition significantly weakens in the upper swash area, where the new bed change profile tends to the reference one.

1
2
3
4
5
6
7
8
9
410 **4. Discussion**

10
11 The study reveals that there is an underestimation of wave run-up and flow
12 depths in the upper swash. This was also noted by Van Rooijen et al. (2012),
13 who used similar equations but with the addition of a diffusion term. Note,
14 however, that in their study infiltration was not included. Here, it is included
15 by default; its exclusion yields water depths in the upper swash and a run-up
16 (not shown) that are closer to those measured (see Fig. 9, 10 and 11). Fig. 15
17 shows a similar effect on the final bed profile for Event 3, and is representa-
18 tive of equivalent results for the other events. In our simulations Event 1 and
19 Event 3 show similar percentage of final void volume occupied by water (21%
20 and 20% respectively). These events possess comparable swash durations (max-
21 imum inundation extent is bigger in Event 3 than in Event 1). The equivalent
22 percentage for Event 5 is 27%, but this event is significantly longer than the
23 other two although showing a smaller inundation, thus meaning that there is a
24 smaller available volume to occupy. Perhaps most pertinent is our lack of knowl-
25 edge of the water table prior to these events. In the absence of any information
26 we assume a perhaps unrealistic scenario in which the water table coincides with
27 bed elevation at $x_s(t_0)$. However, we can see from Fig. 15 that although the
28 inundation is increased by removing infiltration, which is to be expected, as no
29 water is lost on the beach, the resulting bed change is little different from that
30 with infiltration and significantly different from that recorded. So, sensitivity to
31 infiltration is not high, and not likely to account for most of the discrepancies
32 on this sandy beach.
33

34 Event 3 was very depositional in the upper swash (see Fig. 10), and was not
35 well captured by the model, particularly in the upper swash. Assuming that
36 this record is not a result of flotsam deposited at the inundation limit it may
37 be indicative of a large suspended load entrained at the tip of the advancing
38 shoreline, which is not re-entrained in the backwash (see Pritchard & Hogg,
39 2005). This might also point to entrainment by flow turbulence (not included
40 here) as being an important process in achieving good modelling, at least for
41 some swash events. Note also that Event 3 contains two bores, which might
42 also contribute to this notable depositional event.
43

44 If we consider all the events we note that (Fig. 12) in neither Event 1 (deposi-
45 tional) nor in Event 5 (erosional) is the bed change particularly well reproduced.
46 There is, in general, less bed change predicted than is observed. Furthermore,
47 the predicted pattern is consistent: erosion in the lower swash and deposition
48 in the upper, although in differing proportions. The entrainment of sediment
49 as suspended load is governed by m_e , alterations in which primarily affect the
50 magnitude of bed change only, so we are led to the conclusion that this effect is
51 not the primary reason for the discrepancies.
52

53 Sensitivity to $u(x, t_0)$ is notable (see Fig. 16), although much higher initial
54 velocities would be required in order to reproduce observed upper swash hydro-
55 dynamics and bed change for Event 3. The sensitivity noted here can also be
56 viewed as an artefact of the modelling exercise in that we had to consider how to
57 specify these values at $t = t_0$ in the model. These are also linked to the driving
58
59
60
61
62
63
64
65

1
2
3
4
5
6
7
8
9
455 time series $u(x_B, t)$. While our confidence in reproduced u values is reasonably
10 high (see Fig. 12), it is noted that the adopted procedure to estimate $u(x_s(t))$,
11 i.e. reconstruction of the tip velocity from altimeter data, leaves considerable
12 scope for misinterpretation here.

13 The assumed $C(x, t_0)$ profile has a considerable effect on the net bed change
14 (see Fig. 16). This, and $C(x_B, t)$, was unknown to us. If inaccuracies in C are
460 to account for observed discrepancies then they can only do so with a spatially
15 varying $C(x, t_0)$, perhaps with regions of very high concentrations near the
16 tip and much lower values seaward of this. Otherwise net deposition will be
17 predicted everywhere. Note that in our sensitivity analysis we only assumed
18 local equilibrium values for $C(x, t_0)$; much higher values may occur locally,
465 primarily because of turbulence. As mentioned earlier, changed $C(x_B, t)$ values
19 are likely to affect results at most in the lower swash.
20
21
22

23 As mentioned, we did not consider the effect of sediment entrainment / mo-
24 bilisation by turbulence. It could be said that this was considered to some
25 degree by Van Rooijen et al. (2012), who included an acceleration term in their
470 (Nielsen, 2002) bed-load transport expression (which therefore enhances trans-
26 port when accelerations are large, at a bore face, for instance, at which location
27 turbulence is likely to exist). Notionally this term is present to provide enhanced
28 bed shear stress for strongly accelerated flows. In our driving signals some bore
29 fronts were captured, and in others not (see Fig. 3 and 12), so it is not clear how
475 much effect including an acceleration effect would have had on our predictions.
30 Nonetheless, it appears possible that this might provide some enhanced onshore
31 sediment movement, which appears to be missing in Events 1 and 3 in some
32 degree (but not Event 5, in which bore fronts clearly are present): see Fig. 13
33 and 12 (lower panel).
480

34 Van Rooijen et al. (2012) also included suspended sediment diffusion, but
35 this is neglected here, because the greatly reduced spatial extents and durations
36 considered are likely to make this term negligible.
37

38 We did not examine the sensitivity of predictions to bed-load transport, using
39 only the standard MPM formula. However, Kelly & Dodd (2010) noted that the
40 pattern of bed change, including the inundation limit, is affected by bed-load
41 transport (see also Zhu & Dodd, 2015). It therefore seems possible that variation
42 of the proportion of bed- to suspended-load might be worth investigating, with
43 the former affecting the erosion deposition pattern and the latter primarily the
44 magnitudes (see above).
490

45 It should also be remembered that although altimeter data revealed very
46 little alongshore difference between measurements, differences in velocities and,
47 indeed, water and bed levels will exist, and will also contribute to discrepancies
48 observed. It is difficult to quantify how large these will be, but we note that our
49 study, and that of Van Rooijen et al. (2012), show generally good modelling in
50 hydrodynamics, wherein most of the discrepancy is likely to occur in the swash.
495

51 Finally note that the vertical accuracy of surface measurements made in the
52 dried swash area for final bed change comparisons, is the order of 1×10^{-3} m
53 (Blenkinsopp et al., 2011). When plotting data and results after a single swash
54 event, the bed changes show maximum amplitudes of around 1×10^{-2} m. As
500
55
56
57
58
59
60
61
62
63
64
65

1
2
3
4
5
6
7
8
9 a consequence, while it is recognised that higher resolution would be beneficial
10 to reduce the uncertainties related to the morphodynamic change, meaningful
11 comparisons with measurements can indeed be made.
12
13
14
15
16
17
18
19
20
21
22
23
24
25
26
27
28
29
30
31
32
33
34
35
36
37
38
39
40
41
42
43
44
45
46
47
48
49
50
51
52
53
54
55
56
57
58
59
60
61
62
63
64
65

1
2
3
4
5
6
7
8
9
10
11
12
13
14
15
16
17
18
19
20
21
22
23
24
25
26
27
28
29
30
31
32
33
34
35
36
37
38
39
40
41
42
43
44
45
46
47
48
49
50
51
52
53
54
55
56
57
58
59
60
61
62
63
64
65

5. Conclusions

505 Three selected events from an accretive tide at Le Truc Vert beach are simulated in the present work, using a fully-coupled 1D numerical solver. Simulated results are then compared to available measured field data and sensitivity to initial conditions and uncertain assumed parameters illustrated. It is shown that in terms of hydrodynamics, results for all three events compare quite well with
510 field data, which provides confirmation that a 1D, depth-averaged description of the swash is reasonable for describing hydrodynamics on this beach (and, by implication, in other circumstances too). It is noted, however, that the maximum run-up / inundation is smaller in all simulations than that measured, in common with previous work of Van Rooijen et al. (2012).

515 The final bed changes, while of similar orders of magnitude, are generally underestimated, in terms of both deposition and erosion, and the predicted pattern—in the absence of pre-suspended sediment, generally erosion further offshore, and deposition onshore—is not always seen in the data. This discrepancy is thought not to be due to inaccurate estimation of parameters (m_e , K_{hyd} and K_n), but more likely due to initial distributions of pre-suspended sediment
520 concentration and velocity. Furthermore, there appears to be scope for further investigation of the effect of sediment entrainment at bore fronts. In addition, it is noted that bed change is confined consistently with the reduced predicted inundation.

525 In the light of previous points, for future field experiments we would advocate—if possible—the adoption of a higher spatial resolution for velocity and concentration sensors, with the twofold aim of reducing uncertainties about initial / boundary conditions and providing spatially comprehensive data for comparison.

530 **Appendix A. Governing Equations**

The complete system of conservation laws with source terms read:

$$\begin{bmatrix} h \\ hu \\ z_b \\ hC \end{bmatrix}_t + \begin{bmatrix} hu \\ hu^2 + \frac{1}{2}gh^2 \\ \xi q_b \\ huC \end{bmatrix}_x = \begin{bmatrix} -w \\ S_g + S_f - uw \\ S_b - \xi S_s \\ S_s \end{bmatrix}, \quad (\text{A.1})$$

where x and t are the independent variables (space and time respectively); g is the gravitational acceleration; h , u , z_b and C are the dependent variables, namely the water depth, the depth-averaged horizontal velocity, the bed level and the depth-averaged suspended sediment concentration in the order.

Additionally, $\xi = 1/(1-p_b)$, where p_b is bed porosity, and q_b is the instantaneous bedload sediment transport, estimated using the Meyer-Peter-Müller formula (Fredsoe & Deigaard, 1993):

$$q_b = 8.0 \text{sign}(u)(\theta - \theta_{crb})^{\frac{3}{2}} [g(s_{rel} - 1)d_{50}^3]^{\frac{1}{2}}, \quad (\text{A.2})$$

where θ is the Shields parameter, i.e. $\theta = (\tau_b/\rho_w)/[g(s_{rel} - 1)d_{50}]$ and θ_{crb} the critical Shields parameter for initiation of bedload motion; d_{50} is the median sediment diameter while s_{rel} the relative density of sediment compared to water; $\text{sign}(u)$ is added to the original formula to account for the oscillating nature of swash hydrodynamics.

Regarding the source terms of System (A.1), w stands for the infiltration velocity of the percolating water into the permeable beach, the seepage properties of which can be described by the hydraulic conductivity of the sediment K_{hyd} . Information about the water table level is needed as well (Dodd et al., 2008). Note that infiltration is assumed to have no effect on sediment dynamics, except that it causes additional settling of suspended sediment due to the water loss. The meaning of remaining symbols is provided below in (A.3), (A.4), (A.5) and (A.6).

$$S_g = -gh \frac{\partial z_b}{\partial x}, \quad (\text{A.3})$$

$$S_f = -\frac{\tau_b}{\rho_w} = -\text{sign}(u)u_f^2, \quad (\text{A.4})$$

$$S_b = \frac{\xi}{\tan\phi} \frac{\partial (|q_b| \frac{\partial b}{\partial x})}{\partial x}, \quad (\text{A.5})$$

$$S_s = E - D = m_e \left(\frac{\tau_b - \tau_{crs}}{\tau_0} \right) - w_s C. \quad (\text{A.6})$$

Firstly, (A.3) shows the geometric source term.

Secondly, (A.4) is the frictional source term, containing the bottom shear stress (τ_b) divided by the water density (ρ_w). This term is also expressed as function of the friction velocity u_f , computed by the bottom boundary layer solver. The latter requires the value for the bed roughness K_n to estimate the height at

1
2
3
4
5
6
7
8
9 which the velocity is assumed to be zero (i.e. $z_0 = K_n/30$) and the von Kar-
10 man's constant $K = 0.41$ (see Briganti et al., 2011).

11 Thirdly, (A.5) represents the bed diffusion source term, where ϕ is the angle
12 of repose of sediment and b the bed change from the initial bathymetry (Dodd
13 et al., 2008).
14

15 Finally, (A.6) stands for the suspended sediment source term, which consists
16 of the difference between erosional (E) and depositional (D) rates. In particu-
17 lar, m_e is the parameter for the erosional rate, τ_{crs} the threshold shear stress
18 for initiation of suspended load motion and τ_0 the reference shear stress value
19 (Pritchard & Hogg, 2005). In the depositional rate, w_s is the effective settling
20 velocity for suspended sediment, following Zhu & Dodd (2015).
21
22
23
24
25
26
27
28
29
30
31
32
33
34
35
36
37
38
39
40
41
42
43
44
45
46
47
48
49
50
51
52
53
54
55
56
57
58
59
60
61
62
63
64
65

Appendix B. TVD-MacCormack solver

Following Dodd et al. (2008), the effects of infiltration are computed at the end of each time step, i.e. using a weakly-coupled approach, after bed and flow variables have been updated through the fully-coupled solver. Once removed the infiltration-related terms, System (A.1) in vectorial form reads

$$\frac{\partial \mathbf{w}}{\partial t} + \frac{\partial \mathbf{F}(\mathbf{w})}{\partial x} = \mathbf{S}, \quad (\text{B.1})$$

where

$$\begin{aligned} \mathbf{w} &= [h, hu, z_b, hC]^T, \\ \mathbf{F} &= \left[hu, hu^2 + \frac{1}{2}gh^2, \xi q_b, huC \right]^T \text{ and} \\ \mathbf{S} &= [0, S_g + S_f, S_b - \xi S_s, S_s]^T. \end{aligned}$$

The TVD-MCC consists of three steps:

$$\mathbf{w}_m^p = \mathbf{w}_m^n - \frac{\Delta t}{\Delta x} (\mathbf{F}_{m+1}^n - \mathbf{F}_m^n) + \Delta t \mathbf{S}_{m+\frac{1}{2}}^n, \quad (\text{B.2})$$

$$\mathbf{w}_m^c = \mathbf{w}_m^n - \frac{\Delta t}{\Delta x} (\mathbf{F}_m^p - \mathbf{F}_{m-1}^p) + \Delta t \mathbf{S}_{m-\frac{1}{2}}^p, \quad (\text{B.3})$$

$$\mathbf{w}_m^{n+1} = \frac{1}{2}(\mathbf{w}_m^p + \mathbf{w}_m^c) + \left(\mathbf{D}_{m+\frac{1}{2}}^n - \mathbf{D}_{m-\frac{1}{2}}^n \right), \quad (\text{B.4})$$

where \mathbf{D} is the TVD-function. n and m identify the values at the generic time step n at cell m , p and c the predictor and the corrector stages in the order. Δt and Δx are the time and spatial steps respectively.

The adopted TVD-function \mathbf{D} is

$$\mathbf{D}_{m+\frac{1}{2}}^n = \frac{\Delta t}{2\Delta x} \sum_{k=1}^4 [(\bar{\alpha}_k \bar{\Psi}(\bar{\lambda}_k) - \bar{\beta}_k \text{sgn}(\bar{\lambda}_k))(1 - |\bar{\nu}_k|)(1 - \bar{\Phi}(\bar{\theta}_k)) \bar{\mathbf{e}}_k], \quad (\text{B.5})$$

with the overbar indicating values at cell interface $m + \frac{1}{2}$, where Roe averages are considered.

$\bar{\lambda}_k$ is k -th eigenvalue of the Jacobian matrix of System (B.1) when expressed in quasi-linear form (see Castro Diaz et al., 2008, for the geometric source term treatment) and $\bar{\mathbf{e}}_k$ the corresponding right eigenvector (see Zhu, 2012, for details on the eigenstructure).

$\bar{\alpha}_k$ is the k -th wave strength, given by:

$$\bar{\alpha}_k = \frac{\Delta h(\bar{\lambda}_a \bar{\lambda}_b - \bar{u}^2 + \bar{c}^2) + \Delta(hu)(2\bar{u} - \bar{\lambda}_a - \bar{\lambda}_b) + \Delta z_b \bar{c}^2}{(\bar{\lambda}_k - \bar{\lambda}_a)(\bar{\lambda}_k - \bar{\lambda}_b)}, \quad (\text{B.6})$$

with $\bar{c} = \sqrt{g\bar{h}}$ and $a \neq k \neq b$ for $k = 1, 2, 3$. For $k = 4$, it is

$$\bar{\alpha}_4 = \Delta h(-\bar{C}) + \Delta(hC). \quad (\text{B.7})$$

Moreover, $\bar{\Psi}(\bar{\lambda}_k)$ is the entropy correction to $\bar{\lambda}_k$. Due to the work of Harten & Hyman (1983), its expression is

$$\begin{aligned}\bar{\Psi}(\bar{\lambda}_k) &= |\bar{\lambda}_k| & \text{if } |\bar{\lambda}_k| \geq \delta, \\ \bar{\Psi}(\bar{\lambda}_k) &= \delta & \text{if } |\bar{\lambda}_k| < \delta,\end{aligned}\tag{B.8}$$

where δ is a non-negative number determined by the relationship below

$$\delta = \max(0, \bar{\lambda}_k - \lambda_{k,m}, \lambda_{k,m+1} - \bar{\lambda}_k).\tag{B.9}$$

$\bar{\beta}_k$ is the k -th wave strength for the source terms, given by:

$$\bar{\beta}_k = \Delta x \frac{\bar{S}_f(2\bar{u} - \bar{\lambda}_a - \bar{\lambda}_b) + (\bar{S}_b - \xi \bar{S}_s)\bar{c}^2}{(\bar{\lambda}_k - \bar{\lambda}_a)(\bar{\lambda}_k - \bar{\lambda}_b)},\tag{B.10}$$

where $a \neq k \neq b$ and for $k = 1, 2, 3$. For $k = 4$, it is

$$\bar{\beta}_4 = \Delta x \bar{S}_s.\tag{B.11}$$

Finally, $\bar{\nu}_k = \bar{\lambda}_k(\Delta t/\Delta x)$ is the local Courant Number and $\bar{\Phi}(\bar{\theta}_k)$ is the flux limiter. In this paper the following Minmod flux limiter is employed:

$$\bar{\Phi}(\bar{\theta}_k) = \max(0, \min(\bar{\theta}_k, 1)),\tag{B.12}$$

with $\bar{\theta}_k$ being a smoothness ratio defined by

$$\bar{\theta}_k = \frac{\dot{\bar{\alpha}}_k}{\bar{\alpha}_k},\tag{B.13}$$

where $\dot{\bar{\alpha}}_k$ is evaluated at $\dot{m} = m + \frac{1}{2} - \text{sgn}(\bar{\lambda}_k)$.

1
2
3
4
5
6
7
8
9
550 **Acknowledgements**

The authors would like to express their gratitude to The University of Nottingham and The University of Bath for providing financial support. Riccardo Briganti is supported by the EPSRC Career Acceleration Fellowship (EP/I004505/1). The authors would like to acknowledge the financial assistance provided by the Australian Research Council (ARC; DP0770118) and the Natural Environment Research Council (NERC; NE/F009275/1) for funding the field experiments. We would like also to thank The University of New South Wales and The University of Plymouth teams for their assistance with the fieldwork.

560
21
22
23 **References**

24
25 Blenkinsopp, C. E., Turner, I. L., Masselink, G., & Russell, P. E. (2011). Swash
26 zone sediment fluxes: field observations. *Coastal Eng.*, *58*, 28–44.

27
28 Briganti, R., Dodd, N., Kelly, D. M., & Pokrajac, D. (2012a). An efficient and
29 flexible solver for the simulation of the morphodynamics of fast evolving flows
30 on coarse sediment beaches. *Int. J. Numerical Meth. Fluids*, *69*, 859–877.

31
32 Briganti, R., Dodd, N., Pokrajac, D., & O’Donoghue, T. (2011). Nonlinear shallow
33 water modelling of bore-driven swash: description of the bottom boundary
34 layer. *Coastal Eng.*, *58*, 463–477.

35
36 Briganti, R., Dodd, N., Pokrajac, D., & O’Donoghue, T. (2012b). Numerical
37 and experimental description of the flow, boundary layer, and bed evolution
38 in bore-driven swash on a coarse sediment beach. In *Proc. 33rd Int. Conf.*
39 *Coastal Eng.*. Shanghai: A.S.C.E. volume 33.

40
41 Brocchini, M., & Dodd, N. (2008). Nonlinear shallow water equation modeling
42 for coastal engineering. *ASCE J. Water. Port Coast. Ocean Eng.*, *134*, 104–
43 120.

44
45 Castro Diaz, M. J., Fernandez-Nieto, E. D., & Ferreiro, A. M. (2008). Sedi-
46 ment transport models in shallow water equations and numerical approach
47 by higher order finite volume methods. *Computers and fluids*, *37*, 299–316.

48
49 De Melo Apoluceno, D., Howa, H., Dupuis, H., & Oggian, G. (2002). Mor-
50 phodynamics of ridge and runnel systems during summer. *J. Coastal Res.*,
51 *Special Issue 36*, 222–230.

52
53 Dodd, N., Stoker, A., Calvete, D., & Sriariyawat, A. (2008). On the evolution
54 of beach cusps. *J. Fluid Mech.*, *597*, 145–169.

55
56 Fredsøe, J., & Deigaard, R. (1993). *Mechanics of Coastal Sediment Transport*
57 volume 3 of *Advanced Series on Ocean Engineering*. Singapore: World Sci-
58 entific.

- 1
2
3
4
5
6
7
8
9 Harten, A., & Hyman, J. M. (1983). Self adjusting grid methods for one-
10 dimensional hyperbolic conservation laws. *J. Comput. Phys.*, 50, 235–269.
11
12 590 Hibberd, S., & Peregrine, D. H. (1979). Surf and run-up on a beach: A uniform
13 bore. *J. Fluid Mech.*, 95, 323–345.
14
15 Kelly, D. M., & Dodd, N. (2010). Beach face evolution in the swash zone. *J.*
16 *Fluid Mech.*, 661, 316–340.
17
18 Kikkert, G., O’Donoghue, T., Pokrajac, D., & Steenhauer, K. (2013). Exper-
19 595 imental study of bore-driven swash hydrodynamics on impermeable rough
20 slopes. *Coastal Eng.*, 79, 42–56.
21
22 Masselink, G., Russell, P., Turner, I., & Blenkinsopp, C. (2009). Net sediment
23 transport and morphological change in the swash zone of a high-energy sandy
24 beach from swash event to tidal cycle time scales. *Mar. Geol.*, 267, 18–35.
25
26 600 Nielsen, P. (2002). Shear stress and sediment transport calculations for swash
27 zone modelling. *Coastal Engineering*, 45, 53–60.
28
29 O’Donoghue, T., Pokrajac, D., & Hondebrink, L. J. (2010). Laboratory and
30 numerical study of dambreak-generated swash on impermeable slopes. *Coastal*
31 *Eng.*, 57, 513–530.
32
33 605 Packwood, A. R. (1983). The influence of beach porosity on wave uprush and
34 backwash. *Coastal Eng.*, 7, 29–40.
35
36 Packwood, A. R., & Peregrine, D. H. (1980). The propagation of solitary waves
37 and bores over a porous bed. *Coastal Eng.*, 3, 221–242.
38
39 Postacchini, M., Brocchini, M., Mancinelli, A., & Landon, M. (2012). A multi-
40 610 purpose, intra-wave, shallow water hydro-morphodynamic solver. *Adv. Water*
41 *Resources*, 38, 13–26.
42
43 Pritchard, D., & Hogg, A. J. (2005). On the transport of suspended sediment
44 by a swash event on a plane beach. *Coastal Eng.*, 52, 1–23.
45
46 615 S n chal, N., & Arduin, F. (2008). ECORS Truc Vert’08: a multi-institutional
47 international nearshore field experiment. In *AGU Fall Meeting Abstracts*
48 (p. 02). volume 1.
49
50 Soulsby, R. L. (1997). *Dynamics of marine sands. A manual for practical ap-*
51 *plications*. SR 466 Hydraulics Research Wallingford Wallingford, England.
52
53 620 Steenhauer, K., Pokrajac, D., & O’Donoghue, T. (2012). Numerical model
54 of swash motion and air entrapment within coarse-grained beaches. *Coastal*
55 *Eng.*, 64, 113–126.
56
57 Turner, I. L., Russell, P. E., & Butt, T. (2008). Measurement of wave-by-wave
58 bed-levels in the swash zone. *Coastal Eng.*, 55, 1237–1242.
59
60
61
62
63
64
65

- 1
2
3
4
5
6
7
8
9 Van Rijn, L. C. (1982). Equivalent roughness of alluvial bed. *ASCE J. Hydraulic*
10 625 *Eng.*, 108, 1215–1218.
11
12 Van Rijn, L. C. (1984). Sediment transport. Part II: Suspended-load transport.
13 *ASCE J. Hydraulic Eng.*, 110, 1613–1641.
14
15 Van Rijn, L. C. (2007). Unified view of sediment transport by currents and
16 waves. I: Initiation of motion, bed roughness, and bed-load transport. *ASCE*
17 630 *J. Hydraulic Eng.*, 133, 649–667.
18
19 Van Rooijen, A., Reniers, A., Van Thiel de Vries, J., Blenkinsopp, C., & McCall,
20 R. (2012). Modeling swash zone sediment transport at Truc Vert Beach. In
21 *Proc. 33rd Int. Conf. Coastal Eng.*. volume 33.
22
23 Zhang, Q., & Liu, P. L. (2008). A numerical study of swash flows generated by
24 635 bores. *Coastal Eng.*, 55, 1113–1134.
25
26 Zhu, F. (2012). *1D Morphodynamical modelling of swash zone beachface evolu-*
27 *tion*. Ph.D. thesis Department of Civil Engineering, University of Nottingham
28 Nottingham, UK.
29
30 Zhu, F., & Dodd, N. (2015). The morphodynamics of a swash event on an
31 640 erodible beach. *J. Fluid Mech.*, 762, 110–140.
32
33
34
35
36
37
38
39
40
41
42
43
44
45
46
47
48
49
50
51
52
53
54
55
56
57
58
59
60
61
62
63
64
65